Indian Journal of Pure & Applied Physics
Vol. 56, July 2018, pp. 509-521

Structural study, NCA, FTIR, FT-Raman spectral investigations, NBO analysis and thermodynamic functions of N-benzyloxy carbonyl-L-alanine

B Raja[a], V Balachandran[b]*, B Revathi[b] & K Anitha[c]

[a]Department of Physics, Government Arts College, Kulithalai 639 120, India

[b]Research Department of Physics, A A Government Arts College, Musiri 621 211, India

[c]Department of Physics, Bharathidasan University Constituent College, Tiruchirappalli 621 601, India

Received 19 March 2017; accepted 21 August 2017

The FTIR and FT-Raman spectra of N-benzyloxy carbonyl-L-alanine have been recorded and analyzed. Natural bond orbital analysis has been carried out for various intra-molecular interactions that are responsible for the stabilization of the molecule. HOMO-LUMO energy gap has been computed with the help of density functional theory. The statistical thermodynamic functions (heat capacity, entropy, vibrational partition function and Gibbs energy) have been obtained for the range of temperature 100-1000 K. The infrared and Raman spectra have been also predicted from the calculated intensities. Comparison of the experimental and theoretical spectra values provides important information about the ability of the computational method to describe the vibrational modes. In addition to these, Mulliken's atomic charges associated with each atom have also been reported and mapped molecular electrostatic potential (MEP) surfaces have also been performed with the same level of DFT.

Keywords: N-benzyloxyl carbonyl-L-alanine, Vibrational spectra, NBO, HOMO-LUMO, MEP surface

1 Introduction

The understanding of the structure and conformational preference of the zwitterionic form of amino acids is of major interest because it is the form found in biological media[1-5]. This point is important in order to understand protein folding, which is based on the hydrophilic and hydrophobic interactions that determine H-bonding networks. Naturally occurring amino acids have a large conformational flexibility and computational studies should correctly determine the statistical populations found in the experimental data.

This essential amino acid is nonpolar because of the hydrophobic nature of the phenyl group. L-Phe is one of the 20 amino acids used in the formation of proteins and it is a precursor of tyrosine which is important in the synthesis of neuro-transmitters such as dopamine, adrenaline, noradrenalin, and so on. L-Phe cannot be synthesized by the human organism, and so it is important to obtain from the daily die[6-16].

L-alanine is an important reactant for glucagon because it will stimulate its production when his blood sugar is too low. Additionally, it will support the generation of glucose from other amino acids[13]. Studies have shown that prostate fluid has a high concentration of L-alanine may, therefore protect the prostate gland itself from an irregular enlargement. A symptom of this is usually severe pain and problems during urination. This can usually be reduced by the consumption of dietary supplements containing L-alanine. It is therefore assumed that L-alanine can reduce the swelling of the gland's tissue and even be used to treat prostate cancer[14]. A study showed in 2002 that there is an interrelationship between L-alanine and the secretion of insulin by the pancreas. When allowed to react with glucose it leads to an increased production and excretion of glucose therefore positively influencing diabetes. The metabolism of glucose is improved overall and symptoms can be reduced or eliminated altogether[15]. This reduces possible complications of secondary conditions resulting from diabetes, significantly improving patients quality of life. A separate study was able to show that the supplementation of L-alanine is able to increase physical fitness when combined with exercise and protect from cardiovascular illnesses. Over 400 individuals were asked to consume L-Alanine supplements or placebos and the former group was shown to perform significantly better at exercise whilst displaying lower

*Corresponding author (E-mail: brsbala@rediffmail.com)

fat readings in the blood[16]. L-alanine plays a significant role in several metabolic processes and in regulating blood sugar. It can, therefore be used not only against acute low sugar shocks but is also able to stimulate insulin excretion in the pancreas and in doing so significantly improve the metabolism of glucose over longer periods of time.

Literature survey reveals that to the best of our knowledge, the results based on Quantum chemical calculations, FTIR and FT-Raman spectral analyses on NBCLA have no reports. Here we reported detailed interpretations of the infrared and Raman spectra based on the theoretical results, which are acceptable and supportable to each other.

In the present work, we have attempted to interpret the vibrational spectra of NBCLA by using B3LYP level of theory throughout with the cc-pVDZ, 6-31+G(d) basis sets are implemented in the Gaussian 09 program suite[17].

2 Experimental Details

The compound under investigation namely NBCLA was provided by Lancaster Chemical Company, UK, which is of spectroscopic grade (98%) and hence used for recording the spectra as such without any further purification. The room temperature Fourier transform infrared spectrum of the title compound was measured in the 4000-500 cm^{-1} region at a resolution of ±1 cm^{-1} using a BRUKER IFS-66V FT-IR spectrometer equipped with a cooled MCT detector for the mid-IR range. A KBr pellet was used in the spectral measurements. The FT-Raman spectrum of NBCLA was recorded on a BRUKER IFS-66V model interferometer equipped with an FRA-106 FT-Raman accessory in the 3500-0 cm^{-1} Stokes region using the 1064 nm line of a Nd:YAG laser for excitation operating at 200Mw power.

3 Computational Methods

The optimized molecular structure of the title compound and corresponding vibrational harmonic frequencies were calculated by using DFT with Becke3-Lee-Yang-Parr (B3LYP) combined with cc-pVDZ and 6-31+G(d) basis sets using GAUSSIAN 09 program package[17] without any constraint on the geometry. The harmonic vibrational frequencies have been analytically calculated by taking the second-order derivative of energy using the same level of theory. The transformation of force field from Cartesian to symmetry coordinate, the scaling, the subsequent normal coordinate analysis, calculations of PED, IR and Raman intensities were done on a PC with the version V7.0-G77 of the MOLVIB program written by Sundius[18]. To achieve a close agreement between observed and calculated frequencies, the least square fit refinement algorithm was used. By combining the results of the GAUSSVIEW[19] program with symmetry considerations, along with the available related molecules, vibrational frequency assignments were made with a high degree of accuracy. The Raman activities (Si) calculated by Gaussian 09 program have been converted to relative Raman intensities (Ii) using the following relationship derived from the basic theory of Raman scattering[20, 21]:

$$I_i = \frac{f(\nu_0 - \nu_i)^4 s_i}{\nu_i [1 - \exp(\frac{-hc\nu_i}{kt})]} \quad \ldots (1)$$

where ν_0 is the exciting wave number (cm^{-1} units ν_i is the vibrational wavenumber of the i^{th} normal mode, h, c and k are universal constant and f is a suitably chosen common normalization factor for all peak intensities.

4 Results and Discussion

4.1 Molecular geometry

The molecular structure of NBCLA along with numbering of atoms is shown in Fig. 1. The maximum number of potentially active observable fundamentals of a non-linear molecule that contains N atoms is equal to (3n-6), apart from three translational and three rotational degrees of freedom[22]. NBCLA having 29 atoms with 81 Normal modes of vibrations which are distributed amongst the symmetry species as (3N-6) $_{vib}$=55A' (in-plane) + 26" (out-of-plane). The A' vibrations are totally symmetric and give rise to polarized Raman lines whereas A" vibrations are antisymmetric and give rise to depolarized Raman lines. Figures 2 and 3 shows the observed and

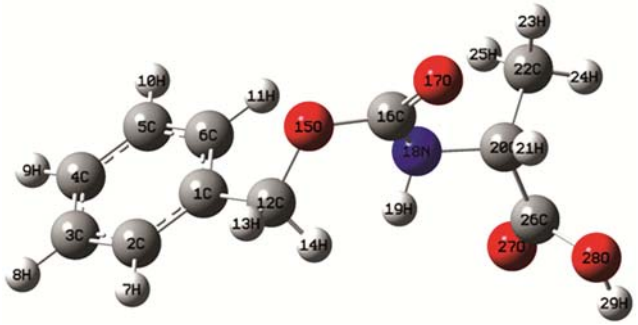

Fig. 1 – Optimized geometrical structure and atomic labeling of N-benzyloxy carbonyl-L-alanine.

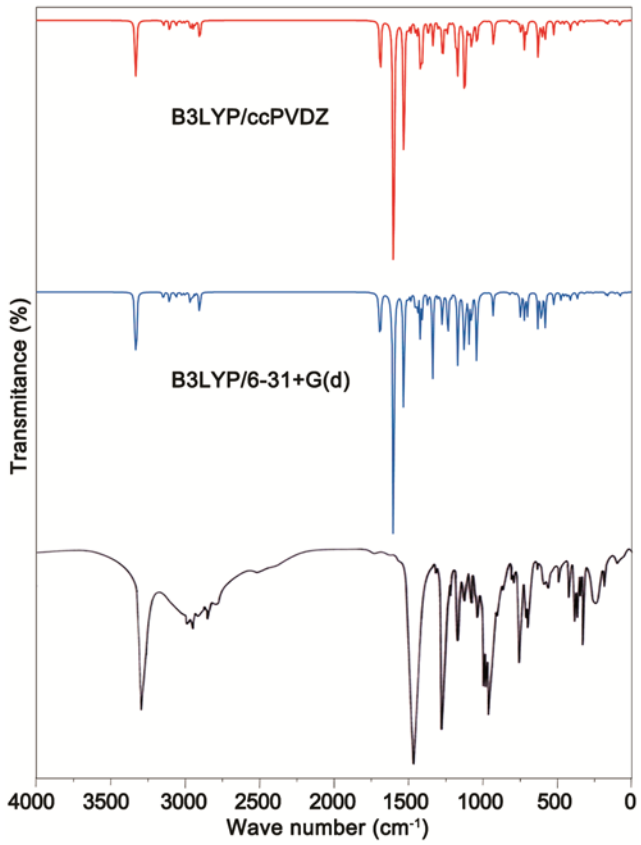

Fig. 2 – Observed and simulated FTIR spectra of N-benzyloxy carbonyl-L-alanine.

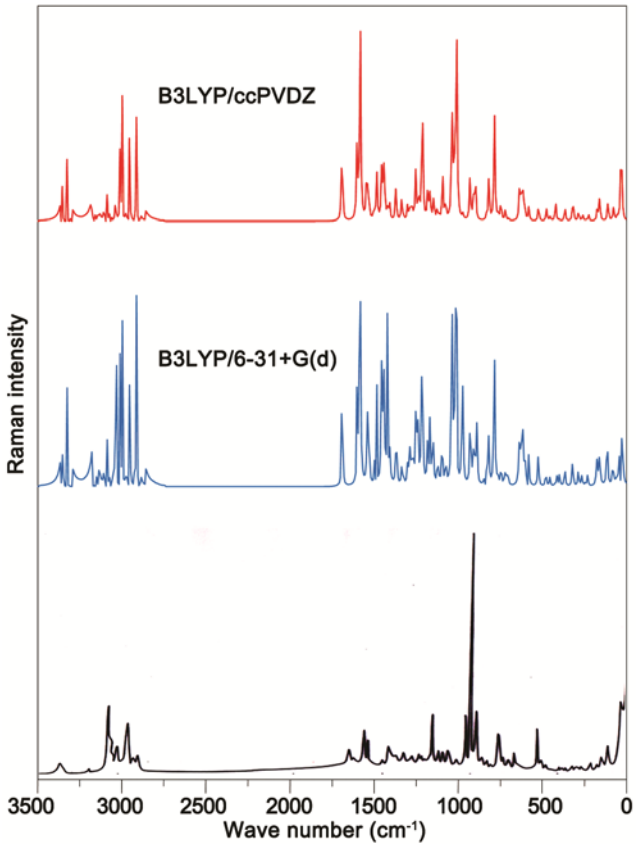

Fig. 3 – Observed and simulated FT- Raman spectra of N-benzyloxy carbonyl-L-alanine.

calculated B3LYP/cc-pVDZ and B3LYP/6-31+G(d) FTIR and FT-Raman spectra of NBCLA, respectively.

The most optimized geometrical parameters (bond length, bond angle and dihedral angle) were calculated by B3LYP/cc-pVDZ and B3LYP/6-31+G(d) basis sets, which are depicted in Table 1.

4.2 Vibrational assignments

The detailed vibrational analysis of fundamental modes of NBCLA along with the FTIR and FT-Raman experimental frequencies and the unscaled and scaled vibrational frequencies using B3LYP/cc-pVDZ and B3LYP/6-31+G(d) basis sets are presented in Table 2.

4.3 N-H vibrations

According to Bellamy[23], the N-H stretching vibrations of aromatic compounds occur in the region 3500-3000 cm^{-1}. The FT-Raman bands observed at 3328 cm^{-1} are assigned to N-H stretching modes of vibrations. The IR and Raman bands at 1240 and 1235 cm^{-1} have been assigned to N-H in-plane bending vibrational modes. The FT-Raman bands are observed at 420 cm^{-1} IS assigned to N-H out-of-plane bending vibrations. The N-H out-of-plane bending vibrations are identified at 423 and 421 cm^{-1}. These vibrations show good agreement with computed harmonic frequency as well as with recorded spectral data.

4.4 CH vibrations

The assignments of the carbon-hydrogen stretching modes are straight forward on the basis of the B3LYP/cc-pVDZ and 6-31+G(d) predicted wavenumbers. The NBCLA molecule gives rise to six C-H stretching, six C-H in-plane bending and six C-H out-of-plane bending vibrations. Aromatic compounds commonly exhibit multiple weak bands in the region 3100-3000 cm^{-1} due to aromatic C-H stretching vibration[24]. The aromatic C-H stretching vibrations are observed in the region 3147, 3105, 3063, 3043, 3021 cm^{-1} is in agreement with recorded FTIR and FT-Raman spectrum at 3044, 2932 cm^{-1}. The six C−H in-plane bending vibrations appear in the range 1000-1300 cm^{-1} in the substituted benzenes and the six out-of-plane bending vibrations occur in the wave number range 750-1000 cm^{-1} are usually weak. The

Table 1 – Optimized geometrical parameters of N-benzyloxy carbonyl-L-alanine by B3LYP/ccPVDZ and B3LYP/6-31+G(d).

Bond length			Bond angle				Dihedral angle		
Parameters	B3LYP/ ccPVDZ	B3LYP/ 6-31+G(d)	Parameters	B3LYP/ ccPVDZ	B3LYP/	6-31+G(d)	Parameters	B3LYP/ ccPVDZ	B3LYP/ 6-31+G(d)
C1-C2	1.40	1.40	C2-C1-C6	119.11		119.13	C6-C1-C2-C3	-0.48	-0.32
C1-C6	1.40	1.40	C2-C1-C12	120.47		120.32	C6-1C-C2-H7	179.15	179.47
C1-12	1.52	1.52	C6-C1-C12	120.38		120.51	C12-C1-C2-C3	177.43	177.60
C2-C3	1.40	1.40	C1-C2-3C	120.54		120.56	C12-C1-C2-H7	-2.94	-2.60
C2-H7	1.09	1.09	C1-C2-H7	119.77		119.85	C2-C1-C6-C5	0.23	0.00
C3-C4	1.40	1.40	C3-C2-H7	119.69		119.59	C2-C1-C6-H11	-179.23	-179.39
C3-H8	1.09	1.09	C2-C3-C4	120.03		120.00	C12-C1-C6-C5	-177.68	-177.92
C4-C5	1.40	1.40	C2-C3-H8	119.76		119.74	C12-C1-C6-H11	2.85	2.69
C4-H9	1.09	1.09	C4-C3-H8	120.21		120.26	C2-C1-C12-H13	-100.47	-104.72
C5-C6	1.40	1.40	C3-C4-C5	119.72		119.73	C2-C1-C12-H14	18.36	14.73
C5-H10	1.09	1.09	C3-C4-H9	120.15		120.15	C2-C1-C12-C15	143.73	139.84
C6-H11	1.09	1.09	C5-C4-H9	120.14		120.12	C6-C1-C12-H13	77.42	73.18
C12-H13	1.10	1.09	C4-C5-C6	120.26		120.25	C6-C1-C12-H14	-163.75	-167.37
C12-H14	1.10	1.10	C4-C5-H10	120.00		120.03	C6-C1-C12-C15	-38.38	-42.26
C12-O15	1.44	1.44	C6-C5-H10	119.74		119.73	C1-C2-C3-C4	0.33	0.34
O15-H16	1.37	1.37	C1-C6-C5	120.34		120.33	C1-C2-C3-C8	179.83	179.81
C16-O17	1.21	1.22	C1-C6-H11	119.28		119.43	H7-C2-C3-C4	-179.30	-179.45
C16-N18	1.37	1.37	C5-C6-H11	120.38		120.24	H7-C2-C3-H8	0.20	0.02
N18-H19	1.01	1.01	C1-C12-H13	110.04		110.44	C2-C3-C4-C5	0.08	-0.03
N18-C20	1.45	1.45	C1-C12-H14	110.93		111.18	C2-C3-C4-H9	179.77	179.74
C20-H21	1.10	1.09	C1-C12-O15	113.84		113.96	H8-C3-C4-C5	-179.42	-179.50
C20-C22	1.54	1.54	H13-C12-H14	107.50		107.66	H8-C3-C4-H9	0.27	0.27
C20-C26	1.52	1.52	H13-C12-O15	103.62		103.06	C3-C4-C5-C6	-0.33	-0.30
C22-H23	1.10	1.09	H14-C12-O15	110.49		110.08	C3-C4-C5-H10	179.73	179.86
C22-H24	1.10	1.09	C12-O15-C16	121.05		122.28	H9-C4-C5-C6	179.98	179.93
C22-H25	1.10	1.10	O15-C16-O17	119.32		119.28	H9-C4-C5-C10	0.05	0.09
C26-O27	1.21	1.21	O15-C16-N18	116.70		116.97	C4-C5-C6-C1	0.17	0.31
C26-O28	1.35	1.35	O17-C16-N18	123.97		123.73	C4-C5-C6-H11	179.63	179.70
O28-H29	0.98	0.98	C16-N18-19	122.60		121.77	H10-C5-C6-C1	-179.89	-179.84
			C16-N18-C20	120.32		120.24	H10-C5-C6-H11	-0.43	-0.46
			19-N18-C20	1O15.87		116.35	C1-C12-O15-C16	-80.64	-79.59
			N18-C20-H21	108.62		108.16	C13-C12-O15-C16	O159.85	160.71
			N18-C20-C22	113.66		113.32	C14-C12-O15-C16	44.96	46.10
			N18-C20-C26	107.15		107.64	C12-O15-C16-O17	-170.00	-169.78
			H21-C20-C22	108.21		108.56	C12-O15-C16-N18	8.75	9.09
			H21-C20-C26	108.31		108.71	O15-C16-N18-H19	13.51	14.29
			C22-C20-C26	110.76		110.35	O15-C16-N18-C20	-179.55	179.16
			C20-C22-H23	108.51		108.60	O17-C16-N18-H19	-167.81	-166.89
			C20-C22-H24	110.50		110.65	O17-C16-N18-C20	-0.87	-2.02
			C20-C22-H25	110.63		110.74	C16-N18-C20-H21	47.62	43.56
			H23-C22-H24	109.12		108.82	C16-N18-C20-C22	-72.89	-76.84
			H23-C22-H25	109.10		109.01	C16-N18-C20-C26	164.41	160.86
			H24-C22-H25	108.95		108.98	H19-N18-C20-H21	-144.60	-O150.78
			C20-C26-O27	125.09		125.21	H19-N18-C20-C22	94.89	88.82
			C20-C26-O28	111.75		111.78	H19-N18-C20-C26	-27.80	-33.48
			O27-C26-O28	123.15		122.98	N18-C20-C22-H23	59.77	58.75
			C26-O28-H29	106.35		107.52	N18-C20-C22-H24	179.36	178.13

(*Contd*.)

Table 1 – Optimized geometrical parameters of N-benzyloxy carbonyl-L-alanine by B3LYP/ccPVDZ and B3LYP/6-31+G(d). (*Contd*.)

Parameters	Bond length		Parameters	Bond angle		Parameters	Dihedral angle	
	B3LYP/ ccPVDZ	B3LYP/ 6-31+G(d)		B3LYP/ ccPVDZ	B3LYP/ 6-31+G(d)		B3LYP/ ccPVDZ	B3LYP/ 6-31+G(d)
						N18-C20-C22-H25	-59.89	-60.91
						H21-C20-C22-H23	-60.97	-61.42
						H21-C20-C22-H24	58.62	57.95
						H21-C20-C22-H25	179.37	178.91
						C26-C20-C22-H23	-179.55	179.53
						C26-C20-C22-H24	-59.95	-61.09
						C26-C20-C22-H25	60.80	59.87
						N18-C20-C26-O27	12.51	17.43
						N18-C20-C26-O28	-168.97	-164.45
						H21-C20-C26-O27	129.51	134.37
						H21-C20-C26-O28	-51.96	-47.51
						C22-C20-C26-O27	-111.97	-106.68
						C22-C20-C26-O28	66.55	71.44
						C20-C26-O28-H29	-177.81	-177.45
						O27-C26-O28-H29	0.75	0.72

Table 2 – Vibrational assignments of fundamental observed frequencies and calculated frequencies of N-benzyloxy carbonyl-L-alanine by B3LYP/ccPVDZ and B3LYP/6-31+G(d).

Mode No.	Symmetry species	Observed frequencies		Calculated frequencies				Infrared intensities		Raman intensities		Vibrational assignments/ (%)
				Unscaled		Scaled						
		FT IR	FT-Raman	B3LYP/ ccPVDZ	B3LYP/ 6-31+G(d)	B3LYP/ ccPVDZ	B3LYP/ 631+G(d)	B3LYP/ ccPVDZ	B3LYP/ 631+G(d)	B3LYP/ ccPVDZ	B3LYP/ 6-31+G(d)	
1.	A’	3336		3704	3680	3335	3336	71.11	70.84	61.89	58.82	υOH(99)
2.	A’		3328	3590	3598	3328	3326	74.04	74.25	43.39	44.50	υNH(98)
3.	A’	3147		3203	3211	3145	3146	10.06	13.69	14.12	14.10	υCH(98)
4.	A’	3105		3196	3204	3103	3105	15.86	20.47	15.73	10.03	υCH(99)
5.	A’	3063		3186	3195	3060	3062	13.99	13.55	48.30	48.27	υCH(98)
6.	A’	3043	3044	3176	3185	3044	3044	0.85	0.56	51.60	44.53	υCH(98)
7.	A’	3021		3167	3175	3020	3021	5.16	6.25	21.02	22.94	υCH(96)
8.	A’		3000	3150	3154	3001	3000	3.71	5.12	29.68	28.53	$\upsilon CH_{3\ asym}$(98)
9.	A’	2966		3127	3135	2964	2965	18.82	20.97	40.07	38.35	$\upsilon CH_{3\ asym}$(98)
10.	A’	2948	2950	3088	3108	2945	2950	13.65	11.29	68.17	62.43	$\upsilon CH_{2\ asym}$(96)
11.	A’		2932	3069	3102	2930	2932	8.03	3.92	43.20	37.16	υCH(98)
12.	A’	2904	2906	3044	3060	2903	2905	13.12	11.00	73.07	90.96	$\upsilon CH_{3\ sym}$(97)
13.	A’			3037	3060	2900	2901	27.26	29.95	73.03	55.12	$\upsilon CH_{2\ sym}$(96)
14.	A’	1690	1691	1826	1812	1690	1691	118.82	181.43	14.65	26.30	υC=O(78), δOH(20)
15.	A’		1602	1810	1787	1600	1601	582.51	638.86	10.88	29.04	υC=O(75), δCN(18)
16.	A’	1582	1580	1657	1656	1584	1582	0.78	0.71	59.49	69.01	υCC(76), δCH(18)
17.	A’		1545	1636	1637	1540	1543	0.12	0.07	15.85	21.93	υCC(75), δCH(21)
18.	A’	1532		1532	1552	1530	1530	305.78	236.13	9.15	7.47	υCN(75), δNH(22)
19.	A’		1500	1524	1540	1500	1501	16.11	9.77	1.19	3.79	υCC(76), δCH(22)
20.	A’	1484		1484	1525	1483	1484	15.93	10.42	2.57	18.44	$\delta CH_{3\ ipb}$(80)
21.	A’		1454	1475	1522	1455	1453	15.22	22.99	30.06	27.26	$\delta CH_{2\ sciss}$ (82)
22.	A’	1442		1472	1511	1443	1440	20.84	77.12	29.34	25.74	$\gamma CH_{3\ opb}$(80)
23.	A’		1421	1461	1495	1420	1421	65.30	8.04	43.60	4.05	υCC(71), δCH(23)
24.	A’	1408		1413	1431	1410	1409	101.27	53.73	10.05	8.74	$\delta CH_{3\ sb}$ (76)
25.	A’	1368	1372	1390	1419	1368	1370	31.11	19.86	15.18	15.58	$\delta CH_{2\ rock}$(76)
26.	A’	1337		1368	1392	1335	1337	44.11	138.68	5.25	8.92	υCO(68), δCH(20)

(*Contd*.)

Table 2 – Vibrational assignments of fundamental observed frequencies and calculated frequencies of N-benzyloxy carbonyl-L-alanine by B3LYP/ccPVDZ and B3LYP/6-31+G(d). (*Contd.*)

Mode No.	Symmetry species	Observed frequencies		Calculated frequencies				Infrared intensities		Raman intensities		Vibrational assignments/ (%)
				Unscaled		Scaled						
		FT IR	FT-Raman	B3LYP/ ccPVDZ	B3LYP/ 6-31+G(d)	B3LYP/ ccPVDZ	B3LYP/ 631+G(d)	B3LYP/ ccPVDZ	B3LYP/ 631+G(d)	B3LYP/ ccPVDZ	B3LYP/ 6-31+G(d)	
27.	A’		1328	1357	1368	1325	1327	0.41	3.58	1.83	2.47	υCC(69), δCH(23)
28.	A’	1298	1300	1350	1361	1299	1300	13.93	8.24	7.36	7.92	δCH(68), γcc(18)
29.	A’	1284		1333	1350	1285	1284	7.30	6.15	13.36	8.46	υCC(66), δCH(21),
30.	A’		1272	1287	1300	1270	1272	89.80	59.98	9.90	5.64	υCO(68), δCH(20)
31.	A’	1252		1276	1291	1251	1252	8.98	1.21	23.27	24.47	δOH(58), δCH(18)
32.	A’			1234	1244	1240	1235	21.87	94.36	21.02	13.56	δNH(58), δCN(18)
33.	A’	1212	1214	1222	1224	1215	1213	5.29	7.94	52.45	70.30	υCC(70), δCH(25)
34.	A’	1179	1180	1193	1212	1180	1181	44.20	0.13	15.53	17.63	δCH(61), γCN(19), δ_{Ring}(8)
35.	A’			1190	1200	1169	1167	88.53	128.09	22.15	14.88	υCN(60), δNH(58)
36.	A’		1148	1171	1192	1150	1145	0.24	0.49	19.12	14.08	δCH(69), γCC(16)
37.	A’	1127	1126	1166	1162	1125	1126	114.30	147.55	4.09	4.93	υCO(69), δOH(16)
38.	A’	1116		1108	1117	1118	1117	71.00	28.57	5.03	3.26	υCC(67), δCH(16)
39.	A’			1102	1109	1095	1093	23.64	81.81	16.80	26.82	δCH(69), γCC(16)
40.	A’	1075	1076	1094	1093	1074	1075	133.29	56.88	8.98	11.09	δC=O(60), δCN(10)
41.	A’	1042		1072	1085	1040	1041	40.47	120.29	24.39	16.89	δCO(60), δCN(10)
42.	A’		1034	1050	1053	1035	1034	9.83	11.48	59.20	70.55	υCC (71), δCH(22)
43.	A’	1021		1023	1026	1020	1021	2.95	2.52	22.89	23.76	δCO(68), γCN(17)
44.	A’	1010	1008	1014	1015	1012	1009	2.63	1.53	38.89	14.66	δRing $_{trigd}$(60), δCC(18), δCH(12)
45.	A’	973		1011	1005	975	973	1.11	0.61	4.10	3.35	δRing $_{asy}$(60), δCC(16), δCH(9)
46.	A’		966	991	985	970	965	0.02	0.25	0.53	0.32	δRing $_{sym}$(60), δCC(12)
47.	A’	931	932	971	970	928	930	53.90	39.71	32.22	32.05	δCN(68)
48.	A’		910	928	927	912	910	1.56	1.97	10.69	15.19	δCH(69), γOH(16)
49.	A’	898		923	921	890	898	0.68	1.14	35.76	35.64	δCN(71), δCO(12)
50.	A’	834	831	865	862	835	832	0.31	0.43	3.40	3.89	δCH(70), δCC(14)
51.	A’		818	836	837	820	818	4.93	3.52	26.96	36.89	δCC(68), δCH(18)
52.	A’	784	784	819	820	785	784	1.69	2.80	8.20	10.56	δCC(65), δCH(20)
53.	A’			771	764	764	761	4.87	2.26	4.20	4.80	δCO(65), δCN(20)
54.	A’	744	746	756	753	745	746	28.40	56.02	11.20	18.46	δCO(62), δCN(21)
55.	A’	720	718	751	751	720	719	47.55	45.40	17.43	10.75	δCC(58), δCH(20)
56.	A”	700		716	707	704	700	26.27	37.46	7.87	1.95	γCH(69), δCC(18)
57.	A”	637		665	662	635	636	8.49	11.01	39.47	34.41	γCH(58), δCC(15)
58.	A”		625	631	632	628	626	66.08	0.47	39.53	39.98	γRing $_{trigd}$(61), γCC(15)
59.	A”	612		629	629	616	613	2.24	77.85	47.05	44.59	γOH(58), δCC(15)
60.	A”		600	624	621	603	601	26.39	24.08	16.24	8.02	δCH$_{3\ ipr}$(76)
61.	A”	582	581	597	600	583	580	40.69	55.81	15.64	18.10	γC=O(78), δOH(15)
62.	A”	522	523	570	569	524	522	23.94	25.64	29.62	23.67	γRing $_{asy}$(61)
63.	A”		475	475	474	479	475	7.20	12.72	14.70	21.98	γCH$_{2wagg}$(76)
64.	A”		454	465	462	455	453	4.98	5.61	10.03	8.92	γC=O(65), δOH(15)
65.	A”		420	426	431	423	421	2.98	67.76	1.95	3.42	γNH(67), γCN(16)
66.	A”		400	407	413	405	400	66.06	2.06	2.31	3.07	γRing $_{sym}$(61)
67.	A”		364	395	394	366	365	8.78	11.76	28.42	33.26	γCN(72), δNH(15)
68.	A”		318	348	345	320	318	2.87	2.52	52.60	73.59	γCH$_{2twist}$(76)
69.	A”		284	310	309	285	284	0.84	0.61	3.88	3.83	γCH$_{3\ opr}$(76)
70.	A”		261	301	298	264	260	1.54	1.45	2.27	2.52	γCH(76)
71.	A”			251	240	245	241	0.24	0.21	8.06	5.94	τCH$_3$(76)
72.	A”		227	234	227	230	225	0.63	0.33	0.64	0.26	γCH(76)
73.	A”			213	206	176	173	4.17	4.74	1.91	1.04	γ CO(60), γNH(16)
74.	A’’		159	192	190	162	159	5.97	6.20	4.60	4.72	γCH(61)
75.	A’’		110	119	119	114	110	2.69	2.43	2.30	2.58	γCH(61), γCC(10)
76.	A’’			83	79	82	80	8.36	2.53	0.58	0.66	γCO(55), γCC(10)
77.	A’’			78	75	75	76	2.80	11.06	0.75	0.73	γCN(57)
78.	A’’			60	55	59	54	1.05	0.91	1.20	1.60	γCO(17), γ CC(52)
79.	A’’			33	34	33	35	0.45	0.69	0.34	0.25	γ CC(58), γ CN(22), γ CO(9)
80.	A’’			32	31	32	30	0.14	0.12	0.79	0.32	γ CC(57), γ CO(18)
81.	A’’			26	25	26	24	0.09	0.04	0.20	0 .05	γ CC(62), γ CH(16)

A’: In-plane; A”: out-of-plane; sym: symmetric stretching; asym: asymmetric stretching; υ:stretching; δ: in-plane bending; γ: out-of-plane bending; τ: torsion; wagg: wagging; sci: scissoring; τ: twisting; sb: symmetric bonding; ipb: in- plane-bending; opb: out-plane-bending; ipr:in-plane-rocking;opr: out-plane-rocking;

C-H in-plane bending vibrations are assigned at 1298, 1179, 834 cm^{-1} in infrared and 1300, 1180, 1148, 910, 831 cm^{-1} in Raman. The computed wave numbers 1299, 1180, 1150, 1095, 912, 835 cm^{-1} are calculated by B3LYP/cc-pVDZ method 1300, 1181, 1145, 1093, 910, 832 cm^{-1} by B3LYP/6- 31+G(d) method. The infrared bands are observed at 700 and 637 cm^{-1} are assigned to C-H out-of-plane bending vibrations. These observed values of C−H vibrations of NBCLA are assigned within the characteristic region and are presented in Table 3.

4.5 CH_3 vibrations

The C-H methyl group stretching vibrations are highly localized and generally observed in the range[25, 26] 3000-2800 cm^{-1}. In the present investigation, the bands with sharp peaks are observed at 2966 and 2904 in FTIR 3000, 2906 and 2956 cm^{-1} are assigned to CH_3 asymmetric and symmetric stretching vibrations. These values are in good agreement with the calculated values. The bands found at 1484, 1440, and 1409 cm^{-1} are assigned to CH_3 in-plane, out-of-plane and symmetric bending vibrations, respectively. The computed values identified at 601 and 284 cm^{-1} are assigned to CH_3 in-plane rock and out-of-plane rock modes of NBCLA molecule. The calculated value at 241 cm^{-1} is assigned to CH_3 twisting vibration of NBCLA molecule. This assignment is also supported by the literature[27].

Table 3 – The charge distribution calculated by the Mulliken and natural bond orbital (NBO) methods using DFT/B3LYP/6-31+G(d) of N-benzyloxy carbonyl-L-alanine molecule.

Atoms	DFT	
	Atomic charges (Mulliken)	Natural charges (NBO)
C1	0.21567	-0.08001
C2	-0.30601	-0.23871
C3	-0.21799	-0.23584
C4	-0.15832	-0.24204
C5	-0.12164	-0.23166
C6	-0.15703	-0.22725
H7	0.18447	0.23966
H8	0.18569	0.24570
H9	0.18271	0.24579
H10	0.18525	0.24702
H11	0.20491	0.25627
C12	-0.39230	-0.09485
H13	0.23572	0.24191
H14	0.21909	0.20407
O15	-0.32070	-0.57089
C16	0.60408	0.93305
O17	-0.49848	-0.58696
N18	-0.47596	-0.70192
H19	0.43445	0.41609
C20	-0.64076	-0.17412
H21	0.25395	0.28131
C22	-0.63241	-0.67592
H23	0.25316	0.25694
H24	0.22748	0.24288
H25	0.22133	0.25431
C26	0.85571	0.79993
O27	-0.46461	-0.60652
O28	-0.57196	-0.71827
H29	0.49449	0.51864

4.6 CH_2 vibrations

For the assignments of CH2 group frequencies, basically six fundamentals can be associated with each CH2 group, namely CH2 symmetric stretch, CH2 asymmetric stretch, CH2 scissoring and CH2 rocking, which belong to in-plane vibrations and two out−of-plane vibrations viz, CH2 wagging and CH2 twisting modes, which are expected to be depolarized[28]. Asymmetric vibrations occur at higher wavenumber compared with the symmetric vibration. The asymmetric CH_2 stretching vibrations are generally observed above 3000 cm^{-1}, while the symmetric stretching will appear between[29] 3000 and 2900 cm^{-1}. In NBCLA the asymmetric stretching vibrations are observed at 2948 cm^{-1} and 2950 cm^{-1} in FTIR and FT-Raman spectrum. The calculated asymmetric vibrations at 2945 cm^{-1} and 2950 cm^{-1} by B3LYP/cc-pVDZ and 6−31+G(d) methods exactly correlate with experimental values.

The scissoring band in the spectrum occurs at a nearly constant position near 1465 cm^{-1}. The band resulting from the methylene rocking vibration in which all of the methylene groups rock in phase appears near 820 cm^{-1}. Absorptions of hydrocarbons due to methylene twisting and wagging vibrations are observed in the region 1350-1150 cm^{-1}. These bands are generally appreciably weaker than those resulting from methylene scissoring[30,31]. The CH_2 scissoring mode was calculated to be 1455 and 1453 cm^{-1} by B3LYP/cc-pVDZ and B3LYP/6−31+G(d) respectively. The FTIR and FT-Raman band at 1368 cm^{-1} and 1372 cm^{-1} represents CH_2 rocking mode. The FT−Raman band at 475 cm^{-1} is assigned to CH_2 wagging mode. The FT−Raman band at 318 cm^{-1} is assigned to CH_2 twisting mode. The calculated CH_2 twisting mode at 320 cm^{-1} and 318 cm^{-1} by

B3LYP/cc-pVDZ and 6−31+G(d) methods exactly correlate with experimental values. Only scissoring is a pure bending mode of vibration. In rocking, wagging and twisting Fermi resonance takes place, resulting in the interaction of C−H deformation vibrations.

4.7 Ring vibrations

The ring stretching vibrations are very prominent, as the double bond is in conjugation with the ring, in the vibrational spectra of benzene and its derivatives[32]. The carbon-carbon stretching vibration occurs in the region of 1650-1200 cm^{-1}. In general, the bands of variable intensity and are observed at 1625-1590, 1590-1575, 1540-1470, 1465-1430 and 1380-1280 cm^{-1} from the frequency range given by Varsanyi[33] for the five bands in the region. In the title molecule, the peaks observed at 1582, 1284, 1212, 1116 cm^{-1} in FT IR and at 1580, 1545, 1214, 1034 cm^{-1} in FT-Raman are ascribed to C-C stretching vibration. The theoretically scaled harmonic frequency values at 1584, 1540, 1285, 1215, 1118 and 1035 cm^{-1} in B3LYP/cc-pVDZ and 1582, 1543, 1284, 1213, 1117, and 1034 cm^{-1} in B3LYP/6-31+G(d) method. The wave numbers are observed in the FT IR spectrum of title molecule at 1008, 966 and 522 cm^{-1} and FT-Raman spectrum at 1014, 991 and 625, 523 and 400 cm^{-1} have been assigned to ring in-plane bending and out-of- plane bending vibrations. The computed values are 1009, 973 and 965 cm^{-1} is assigned to ring in-plane bending vibrations. The bands identified at 626, 522 and 400 cm^{-1} are assigned to ring out-of- plane bending vibrations. The above results show good agreement with experimental observations. Usually, an in-plane deformation vibration is at higher frequencies than that the out-of-plane vibration[34].

4.8 Carboxylic acid group vibrations

Generally, carboxylic acid group containing molecules possesses dimeric character. The carboxylic acid dimer is formed by strong hydrogen bonding in the solid and liquid state. Hence the derivatives of carboxylic acids are best characterized by the carbonyl and hydroxyl groups. The presence of carbonyl group is the most important in the infrared spectrum because of its strong intensity of absorption and high sensitivity towards relatively minor changes in its environment. Intra- and intermolecular hydrogen bonding factors affect the carbonyl and absorptions in common organic compounds due to inductive, mesomeric, field and conjugation effects[35]. The characteristic infrared absorption wavenumbers of C=O in acids are normally strong in intensity and found in the region[36] 1690-1800 cm^{-1}. In the present study, the strong band at 1690 cm^{-1} in FTIR and the band at 1691 cm^{-1} in FT-Raman are assigned to C=O stretching mode. The band observed at 1337 cm^{-1} in FTIR is assigned to C-O stretching mode. The wavenumbers of this mode calculated by DFT is in excellent agreement with the experimental FTIR and FT-Raman wavenumbers.

The O-H stretching vibrations are characterized by a very broad band appearing in the region[37] 3400-3600 cm^{-1}. Hence the band observed at 3336 cm^{-1} in FTIR is assigned to O-H stretching of a carboxylic acid group of NBCLA. The scaled theoretical values, by B3LYP/cc-pVDZ and 6-31+G(d) basis sets, are in good agreement with O-H stretching of similar kind of molecules[38]. The strong band observed at 1252 cm^{-1} in FTIR is assigned to O-H in-plane bending of the carboxylic acid group. In this mode, the TED contribution of C-O stretching is significant.

4.9 CN vibrations

The C-N stretching frequency is a rather hard job since there are problems in identifying these frequencies from other vibrations. The C-N stretching absorption for aromatic amines is identified in the region[39] 1382-1266 cm^{-1}. In the present study, the C-N stretching vibrations are observed only at 1532 cm^{-1} in FT-Raman spectra is good agreement with the experimental values, computed values calculated at 1530 cm^{-1} and 1169, 1167 cm^{-1} in B3LYP/cc-pVDZ and 6-31+G(d) basis sets. According to the literature, one band is more deviated since the C-N bond is in between CO and NH. All the bands lie in the expected range when compared to the literature[40]. Consequently, the C-N in-plane bending vibrations assigned at 931, 898 and 932 cm^{-1} in FTIR and FT-Raman spectra and the C-N out-of-plane bending vibrations assigned at 364 cm^{-1} in FT-Raman spectra. These assignments are validated by the literature[41-43]. The identification of C-N vibration is a difficult task since it falls in a complicated region of the vibrational spectrum. However, with the help of force field calculations, the C-N vibrations were well identified and assigned in this study.

4.10 NBO and second order perturbation analysis

NBO analysis provides the most accurate possible 'natural Lewis structure' picture of φ, because all

orbital details are mathematically chosen to include the highest possible percentage of electron density. The interaction between both filled and virtual orbital spaces information correctly explained by the NBO analysis, it could enhance the analysis of intra and intermolecular interactions. The second-order Fock matrix was carried out to evaluate the donor-acceptor interactions in the NBO analysis[44]. The result of information is a loss of occupancy from the concentrations of the electron NBO of the idealized Lewis structure into non-Lewis orbital. For each donor (i) and acceptor (j), the stabilization energy $E^{(2)}$ associates with the delocalization $i \rightarrow j$ is estimated as:

$$\nabla E_{i-j*}^{(2)} = -2\frac{\left\langle \sigma_i \middle| \hat{F} \middle| \sigma_j^* \right\rangle^2}{\varepsilon_i - \varepsilon_j} = -2\frac{F_{ij}^2}{\Delta E} \quad \ldots (2)$$

The Fock matrix analysis yields different types of donor where $\hat{F}$ is the effective orbital Hamiltonian (Fock operator) and $\langle \sigma_i | \hat{F} | \sigma_j^* \rangle$ and $\langle \sigma_i^* | \hat{F} | \sigma_j^* \rangle$acceptor interactions and their stabilization energy.

Natural bond orbital analysis bonding and interaction among bonds and also investigate charge transfer or conjugative interaction in molecular systems. Some electron donor, acceptor orbital and the interacting stabilization energy resulted from the second- order micro-disturbance theory is reported[45]. The larger the $E^{(2)}$ value, the more intensive is the interaction between electron donors and electron acceptors, i.e., the more donating tendency from electron donors to electron acceptors and the greater the extent of conjugation of the whole system. Delocalization of electron density between occupied Lewis orbital's (bond) and formally unoccupied non-Lewis orbital's (anti-bond) corresponds to a stabilizing donor-acceptor interaction. NBO analysis has been performed on the molecule at the DFT level in order to elucidate the intermolecular, re-hybridization and delocalization of electron density within the molecule. The most important interactions in the title molecule having bond pair-bond pair interaction between bonding $\sigma(N_{18}\text{-}H_{19})$ and anti-bonding $C_{16}\text{-}O_{17}$ to give a strong stabilization of 5.46 kJ/mol, lone pair-bond pair interaction between lone pair(1)N_{18} with that of anti bonding $O_{16}\text{-}C_{17}$, LP(2)O_{27} with that of anti-bonding $C_{26}\text{-}O_{28}$ and lone pair LP(2)O_{28} with that of anti-bonding $C_{26}\text{-}O_{27}$, results the stabilization of 10.70, 31.91 and 46.90 kJ/mol, respectively, which donates larger delocalization. Table 4 list out the calculated second order interaction energies $E^{(2)}$ between the donor-acceptor orbital's in NBCLA molecule with B3LYP/6-31+G(d) method.

4.11 HOMO, LUMO analysis

The most important orbitals in the molecule are the frontier molecular orbitals, called highest occupied molecular orbital (HOMO) and lowest unoccupied molecular orbital (LUMO). These orbitals determine

Table 4 – Second-order perturbation theory analysis of Fock matrix in NBO basic corresponding to the intra molecular bonds of N-benzyloxy carbonyl-L-alanine.

Donor (i)	ED (i) (e)	Acceptor (j)	ED (j) (e)	[a]$E^{(2)}$ (kJ mol^{-1})	[b]$E(j) - E(i)$ (a.u.)	[c]$F(i\text{-}j)$ (a.u.)
$\sigma(C_2\text{–}H_7)$	1.98113	$\sigma^*(C_1\text{–}C_6)$	0.02240	4.62	1.10	0.064
$\sigma(C_3\text{–}H_8)$	1.98255	$\sigma^*(C_4\text{–}C_5)$	0.01573	3.68	1.10	0.057
$\sigma(C_6\text{–}H_{11})$	1.97974	$\sigma^*(C_1\text{–}C_2)$	0.02128	4.68	1.09	0.064
$\sigma(C_{12}\text{–}O_{15})$	1.98235	$\pi^*(C_{16}\text{–}O_{17})$	0.16449	3.13	0.97	0.051
$\sigma(C_{16}\text{–}O_{17})$	1.99526	$\sigma^*(C_{12}\text{–}O_{15})$	0.01992	1.37	0.85	0.031
$\sigma(C_{16}\text{–}N_{18})$	1.98509	$\sigma^*(C_{20}\text{–}C_{26})$	0.06711	1.37	1.09	0.035
$\sigma(N_{18}\text{–}H_{19})$	1.96866	$\sigma^*(C_{16}\text{–}O_{17})$	0.11659	5.46	0.81	0.061
$\sigma(N_{18}\text{–}C_{20})$	1.97778	$\sigma^*(O_{15}\text{–}C_{16})$	0.11145	3.28	0.99	0.052
$\sigma(C_{20}\text{–}H_{21})$	1.97647	$\sigma^*(C_{26}\text{–}O_{27})$	0.02378	5.28	1.09	0.068
$\sigma(O_{28}\text{–}H_{29})$	1.98854	$\sigma^*(C_{25}\text{–}C_{26})$	0.06711	3.87	1.11	0.059
LP(1)O_{15}	1.95597	$\sigma^*(C_{16}\text{–}N_{18})$	0.09378	6.48	0.86	0.067
LP(1)N_{18}	1.83453	$\sigma^*(C_{16}\text{–}O_{17})$	0.11659	10.70	0.74	0.081
LP(1)O_{28}	1.97688	$\sigma^*(C_{26}\text{–}O_{27})$	0.02378	7.26	1.16	0.082
LP(2)O_{15}	1.85692	$\sigma^*(C_{16}\text{–}O_{17})$	0.11659	11.69	0.75	0.084
LP(2)O_{27}	1.85688	$\sigma^*(C_{26}\text{–}O_{28})$	0.09512	31.91	0.61	0.126
LP(2)O_{28}	1.81207	$\pi^*(C_{26}\text{–}O_{27})$	0.21115	46.90	0.33	0.112

[a]$E^{(2)}$ means energy of hyper conjugative interactions.

[b] Energy difference between donor and acceptor i and j NBO orbitals.

[c]$F(i\text{-}j)$ is the Fock matrix element between i and j NBO orbitals.

the way of molecule interacts with other species. The frontier molecular energy gap helps to characterize the chemical reactivity and kinetic stability of the molecule. A molecule with a small frontier orbital gap is more polarizable and is generally associated with a high chemical reactivity, low kinetic stability and is also termed as soft molecule[46]. The low values of the frontier orbital gap in NBCLA make it more chemically reactive and less kinetic stable. The conjugated molecules are characterized by a small highest occupied molecular orbital-lowest unoccupied molecular orbital (HOMO-LUMO) separation, which is the result of a significant degree of intramolecular charge transfer from the end-capping electron acceptor groups through p-conjugated path[47]. The 3D plot of the frontier orbital's HOMO and LUMO of NBCLA molecule is shown in Fig. 4.

The positive phase is red and negative phase one is green. Many organic molecules, conjugated p electrons are characterized by large values of molecular first hyperpolarizabilities, were analyzed by means of vibrational spectroscopy[48,49]. In most cases, even in the absence of inversion symmetry, the strongest band in the FT-Raman spectrum is weak in the FT-IR spectrum vice versa. But the intramolecular charge transfer from the donor-acceptor group in a single-double bond conjugated path can induce large variations of both the dipole moment and the polarizability, making FTIR and FT-Raman activity strong at the same time. This electronic transition absorption corresponds to the transition from the ground to the first excited state and is mainly described by an electron excitation from the HOMO to LUMO. An electron excite from the highest occupied molecular orbital to the lowest unoccupied molecular orbital (HOMO-LUMO).

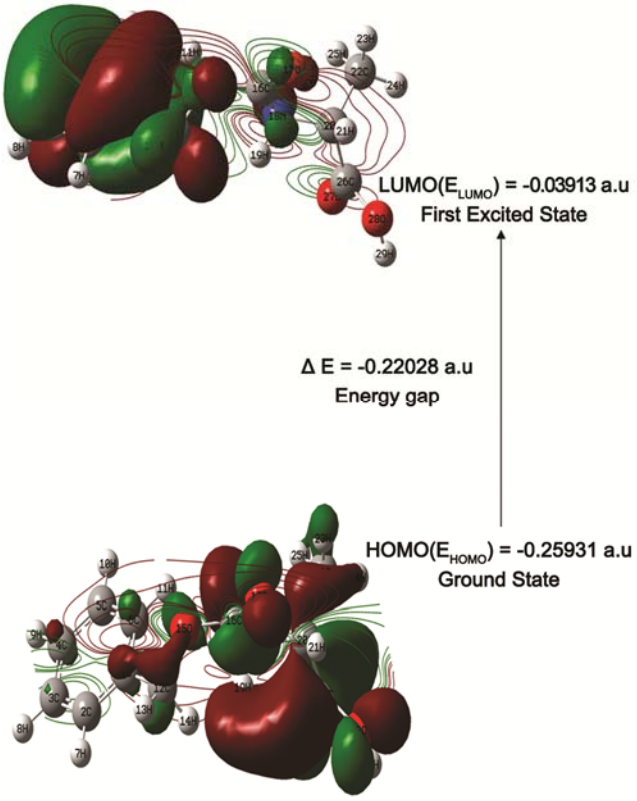

Fig. 4 – Atomic orbital composition of the molecular orbital for N-benzyloxy carbonyl-L-alanine.

Generally, the energy gap between the HOMO and LUMO decreases, it is easier for the electrons of the HOMO to be excited. The higher energy of HOMO, the easier it is for HOMO to donate electrons whereas it is easier for LUMO to accept electrons when the energy of LUMO is low.

HOMO energy = - 0.25931 a.u
LUMO energy = - 0.03913 a.u
Energy gap = -0.22018 a.u

4.12 Mulliken atomic charges

The calculation of atomic charges plays a key role in the application of quantum mechanical calculation to describe the electronic characteristics of molecular systems[50]. A comparative study of the NBO and Mulliken atomic charge distributions in the title molecule, determined on the basis of the quantum mechanical method with the B3LYP method is presented in Table 3.

Regarding the molecular symmetries, only the charges of 29 atoms are listed for NBCLA. The comparison between Mulliken's net charges and the atomic natural one is not an easy task since the theoretical background of the two methods was very different. Looking at the results there are surprising differences between the Mulliken's and the NBO charges. All of the NBO charges have the negative sign for Carbon atom except C16 and C26 atom on the B3LYP method, whilst the Mulliken's values for all the Carbon atoms have the same sign and C1 atom are different in sign as compared to these values for the method.

The natural atomic charge is based on the theory of the natural population analysis. The analysis is carried out with natural bond orbital analysis (NBO). They are linear combinations of the natural atomic orbitals. The derivation of a valence-shell atomic orbital (NAO) involves diagonalization of the localized block of the full density matrix of a given molecule

associated with basic functions on that atom. A distinguishing feature of NAOs is that they meet the simultaneous requirement of orthonormality and maximum occupancy. In a polyatomic molecule the NAOs mostly retain one-center character, and thus they are optimal for describing the molecular electron density around each atomic center. Natural bond orbitals are linear combinations of the NAOs of two bonded atoms. The natural population analysis satisfies Pauli's exclusion principle and solves the basis set dependence problem of the Mullikan's population analysis.

The variations in NBO and Mullikan's charges on the molecular system, in particularly carboxyl and hydroxyl groups in the title molecule may suggest the formation of intermolecular interactions in solid forms.

4.13 Analysis of molecular electrostatic potential (MEP)

The molecular electrostatic potential, $V(r)$, at a given point $r(x, y, z)$ in the vicinity of a molecule, is defined in terms of the interaction energy between the electrical charge generated from the molecule electrons and nuclei and a positive test charge (a proton) located at r. The molecular electrostatic potential (MEP) is related to the electronic density and is a very useful descriptor for determining sites for electrophilic attack and nucleophilic reactions as well as hydrogen-bonding interactions[51,52]. The molecular electrostatic potential surface which is a method of mapping electrostatic potential onto the iso-electron density surface simultaneously displays electrostatic potential (electron + nuclei) distribution, molecular shape, size and dipole moments of the molecule and it provides a visual method to understand the relative polarity[53]. The total electron density and MEP surfaces of N-benzyloxy carbonyl-L-alanine under investigation are constructed by using the B3LYP/6-31+G(d) method. The total electron density surface mapped with the electrostatic potential, the electrostatic potential contour maps for positive and negative potentials, and the electrostatic potential surface of N-benzyloxy carbonyl-L-alanine are shown in Fig. 5, respectively. The color 1 scheme for the MEP surface is: red, electron rich, partially negative charge; blue, electron deficient, partially positive charge; light blue, slightly electron deficient region; yellow, slightly electron-rich region; green, neutral; respectively. The most positive potential lies around the hydrogen of the OH group. The predominance of the light green region in the MEP surfaces corresponds to a potential halfway between the two extremes of red and blue color.

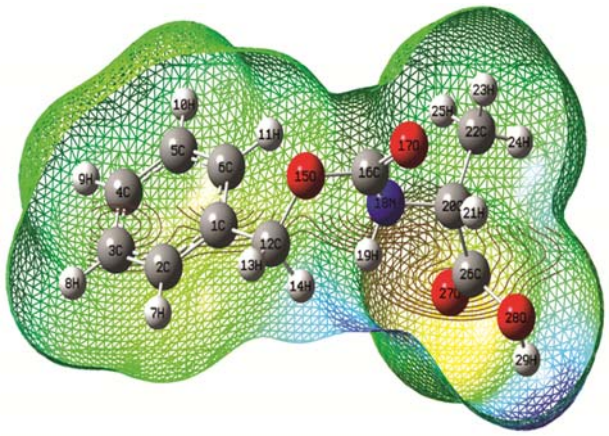

Fig. 5 – DFT (B3LYP)/6-31+G(d) calculated 3D molecular electrostatic potential contour map of N-benzyloxy carbonyl-L-alanine.

4.14 Thermodynamic properties

On the basis of the vibrational analysis, the statically thermodynamic functions: heat capacity (C_p), enthalpy changes (ΔH), Gibb's free energy (ΔG) and entropy (S^0m) for the title molecule were obtained from the theoretical harmonic frequencies and listed in Table 5. From the Table 5, it can be observed that these thermodynamic functions are increasing with temperature ranging from 100 to 1000 K due to the fact that the molecular vibrational intensities increase with temperature. The correlation equations between heat capacity, Gibb's free energy, entropy, enthalpy changes and temperatures were fitted by quadratic formulas and the corresponding fitting factors ($R2$) for these thermodynamic properties are 0.999, 0.999, 0.564 and 0.476, respectively. The corresponding fitting equations are as follows and the correlation graphics of those shown in Fig. 6.

$$\left(Cp^0\right) = 6.437 + 21.00T - 0.864T^2 (R^2 = 0.999)$$

$$(S^0) = 44.28 + 56.03T - 4.472T^2 (R^2 = 0.564)$$

$$(H - E/T) = -15.42 + 41.62T - 4.118T^2 (R^2 = 0.476)$$

$$(G - E/T) = -59.70 - 14.40T + 0..353T^2 (R^2 0.999)$$

All the thermodynamic data supply helpful information for the further study on the NBCLA. They can be used to compute the other thermodynamic energies according to relationships of thermodynamic functions and estimate directions of chemical reactions according to the second law of thermodynamics in thermo chemical field.

Table 5 – Thermodynamic functions of N-benzyloxy carbonyl-L-alanine.

Temperature (K)	C_p (cal mol^{-1} K^{-1})	$(H-E)/T$ (cal mol^{-1} K^{-1})	$(G-E)/T$ (cal mol^{-1} K^{-1})	S (cal mol^{-1} K^{-1})
100	27.93	19.75	-72.34	92.10
200	43.55	41.17	-88.13	129.31
300	60.51	65.36	-100.77	166.13
400	76.83	91.22	-112.14	203.36
500	90.74	118.35	-122.80	241.15
600	102.05	146.49	-132.93	279.42
700	111.22	12.71	-142.59	155.30
800	118.75	15.13	-151.83	166.96
900	125.01	17.99	-160.66	178.66
1000	130.28	21.24	-169.12	190.37

Parameters	B3LYP/6-31+G(d)
Self consistent field energy	-21298.2619 eV
Zero point vibrational energy	145.77724 Kcal/Mol
Rotational constants	0.73244 GHz
	0.34093 GHz
	0.27871 GHz
Entropy	129.963 cal mol^{-1} K^{-1}
Specific heat capacity at constant volume	56.612 cal mol^{-1} K^{-1}
Translational energy	42.110 cal mol^{-1} K^{-1}
Rotational energy	32.802 cal mol^{-1} K^{-1}
Vibrational energy	55.051 cal mol^{-1} K^{-1}

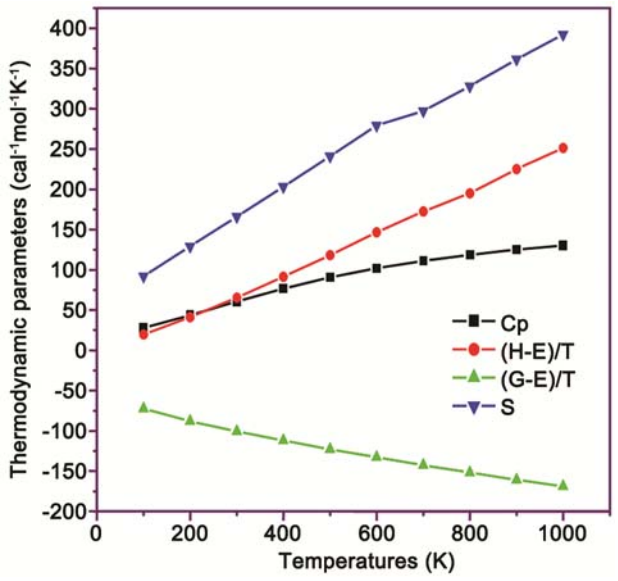

Fig. 6 – Correlation graphic of thermodynamic parameters and temperature for N-benzyloxy carbonyl-L-alanine.

Notice: all thermodynamic calculations were done in the gas phase and they could not be used in the solution.

In addition to the vibrational assignments, several thermodynamic parameters, rotational constants, and dipole moment have been presented in Table 5. The self-consistent field (SCF) energy, zero point vibrational energies (ZPVEs), rotational constants and entropy $S_{vib}(T)$ are calculated to the extent of accuracy and variations in the ZPVEs seem to be insignificant[53]. Dipole moment reflects the molecular charge distribution and is given as a vector in three dimensions. Therefore, it can be used as a descriptor to depict the charge movement across the molecule. The direction of the dipole moment vector in a molecule depends on the centers of positive and negative charges. Dipole moments are strictly determined for neutral molecules. For charged systems, its value depends on the choice of origin and molecular orientation.

5 Conclusions

The present work for the proper vibrational frequency assignments for the compound of NBCLA from the FTIR and FT-Raman spectra have been recorded for the first time. The equilibrium geometries, harmonic vibrational frequencies, IR intensities and Raman intensities of the title compound were determined and analyzed by B3LYP levels of theory utilizing cc-pVDZ and 6-31+G(d) basis sets. Although B3LYP/6-31+G(d) has performed better than cc-pVDZ, as far as the bond lengths are concerned, both the methods have performed nearly to the same level across the bond angle sets. We have carried out density functional theory calculations on the structure, vibrational spectra, NBO, HOMO-LUMO analyses, Mulliken's atomic charges of the compound. On the basis of agreement between the calculated and experimental results assignments of all the fundamental vibrational modes of NBCLA are examined and proposed in this investigation. The lowering of HOMO-LUMO energy gap explains the eventual charge transfer interactions takes place within the molecule. The NBO analysis performed in this study enabled us to know about the conjugative interactions and another type of interactions taking place within the molecular species. The vibrational frequencies were calculated and scaled values have been compared with the experimental FTIR and FT-Raman spectra. The MEP map shows the negative potential sites are an oxygen atom as well as the positive potential sites on the molecule. These sites give information about the region from where the compound can have intra-molecular interactions. The thermodynamic features of the title compound at different temperatures have

been calculated. It is seen that the heat capacities, entropies and enthalpies increase with the increasing temperature owing to the intensities of the molecular vibrations increase with increasing temperature.

Reference

1 Allen J, *Biophysical chemistry,* (Wiley Blackwell: New York), 2008.
2 Jukes T H, *Biochem Biophys Res Commun*, 27 (1967) 573.
3 Bada J L, Galvin D P, McDonald G D & Becker L, *Science*, 279 (1998) 362.
4 Kim T K & Jhon M S, *J Mol Liq*, 59 (1994) 179.
5 Stryer L, Berg J M & Tymoczko J L, *Bioquímica,* 5th Edn, (Editorial Reverte, W H Freeman and Company: New York), 2003.
6 Gonzalez J & Willis M S, *Lab* Med, 41 (2010) 118.
7 Ikeda M, *Adv Biochem Eng Biotechnol*, 79 (2002) 1.
8 Redgrave P & Gurney K, *Nat Rev Neurosci*, 7 (2006) 967.
9 Ben-Jonathan N & Hnasko R, Endocrinol Rev, 22 (2001) 724.
10 Manning G, Whyte D B, Martinez R, Hunter T & Sudarsanam S, *Science*, 298 (2002) 1912.
11 Wang J C, *Annu Rev Biochem*, 54 (1985) 665.
12 J R A Moreno, M M Q Moreno, F P Ureña & J J L González, *Tetrahedron Asymm*, 23 (2012) 1084.
13 Müller W A, *J Clin Invest*, 50 (2001) 2215.
14 Shiga H, Kumaki E & Imamura A, *Hinyokika Kiyo*, 14 (2008) 625.
15 Brennan L, Shine A, Hewage C, Malthouse J P, Brindle M M, McClenaghan N, Flatt P R & Newsholme P, *Diabetes*, 51 (2002) 1714.
16 Walter A A, Smith A E, Kendall K L, Stout J R & Cramer J T, *J Strength Cond Res*, 24 (2010) 1199.
17 Frisch M J, Trucks G W, Schlegal H B, Scuseria G E, Robb M A, Cheesman J R, Zakrzewski V G, Montgomerg J A, Strtmann R E, Burant J C, Dapprich S, Milliam J M, Daniels A D, Kudin K N, Strain M C, Farkas O, Tomasi J, Barone V, Cossi M, Camme R, Mennucci B, Pomelli C, Adamo C, Clifford S, Ochterski J, Petersson G A, Ayala P Y, Cui Q, Morokuma K, Rega N, Salvador P, Dannenberg J J, Malich D K, Rabuck A D, Raghavachari K, Foresman J B, Cioslowski J, Ortiz J V, Baboul A G, Stetanov B B, Liu G, Liashenko A, Piskorz P, Komaromi I, Gomperts R, Martin R L, Fox D J, Keith T, Al- Laham M A, Peng C Y, Nsnsyskkara A, Challacombe M, Gill P M W, Johnson B, Chen W, Wong M W, Andres J L, Gonzalez C, Head-Gordon M, Replogle E S & Pople J A, (*2009) GAUSSIAN 09, Revision A02, Gaussian, Inc MOLVIB,* T Sundius, 2002.
18 Frisch A, Neilson A B & Holder A J, *GAUSSVIEW User Manual, Gaussian, Inc, Pittsburgh, CT*, 2009.
19 Keresztury G, Holly S, Varga J, Besenyei G, Wang A V & Durig J R, *Spectrochim Acta*, 49A (1993) 2007.
20 Keresztury J R, Chalmers J M & Griffith P R, *Raman spectroscopy: Theory, hand book of vibrational spectroscopy, Vol. 1,* (John Wiley and Sons Ltd: New York), 2002.
21 Silverstein M, Clayton Basseler G & Morill C, *Spectrometric identification of organic compound,* (Wiley, New York), 1981.
22 Bellamy L J, *The infrared spectra of complex molecules,* (John Wiley: New York), 1959.
23 Subramanian M K, Anbarsan P M & Manimegalai S, *J Raman Spectrosc*, 40 (2009) 1657.
24 Dollish F R, Fateley W G & Bentely F F, *Characteristic Raman frequencies on organic compounds,* (Wiley: New York), 1997.
25 Silverstein R M, Clayton B G & Morril T C, *Spectroscopic identification of organic compounds*, (John Wiley: New York), 1991.
26 Krishnakumar V & Balachandran V, *Spectrochim Acta Part A*, 61 (2005) 2510.
27 Gunasekaran S, Balaji R A, Kumaresan S, Anand G & Srinivasan S, *Can J Anal Sci Spectrosc*, 53 (2008) 149.
28 Matulkova I, Nemec I, Teubner K, Nemec P & Micker Z, *J Mol Struct*, 873 (2008) 46.
29 Silverstein R M, Bassler C G & Morril T C, *Spectrometric identification of organic compounds,* (Wiley International Edition), 1974.
30 Amalanathan M, Hubert Joe I & Irena K, *J Raman Spectrosc*, 41 (2010) 1076.
31 Varsanyi G, *Vibrational spectra of benzene derivatives,* (Academic Press: New York), 1969.
32 Varsanyi G, *Assignments of vibrational spectra of seven hundred benzene derivatives,* Adam Hilger, 1-2 (1974).
33 Socrates G, *Infrared characteristic group frequencies*, (Wiley Interscience Publication), 1980.
34 Karabacak M, *J Mol Struct*, 919 (2009) 215.
35 Silverstein M, G C Basseler & Morill C, *Spectrometric Identification of Organic Compounds,* (Wiley: New York), 1981.
36 Sharma Y R, *Elementary organic spectroscopy,* (Shoban Lal Nagin Chand & Company, Educational Publishers: New Delhi), 1980.
37 Yulan Z H U, Feng M A, Kuirong M A, Licao & Lianhua Zhao, *J Chem Sci*, 123 (2011) 687.
38 Saravanan S & Balachandran V, *Spectrochim Acta*, 120A (2014) 351.
39 Krishnakumar V & Balachandran V, *Spectrochim Acta*, 61A (2005) 1001.
40 Medhi K C, Barman R & Sharma M K, *Indian J Phys*, 68B (1994) 189.
41 Smith B, *Infrared spectral interpretation, a systematic approach*, (CRC Press, Washington: DC), 1999.
42 Sathyanarayana D N, *Vibrational spectroscopy-theory and applications, 2nd Edn,* (New Age International (P) Limited Publishers: New Delhi), 2004.
43 Chocholousova J, Spirko V & Hobza P, *Phys J Phys Chem*, 6 (2004) 37.
44 James C, Amal Raj A, Reghunathan R, Joe I H & Jayakumar V S, *J Raman Spectrosc*, 37 (2006) 1381.
45 Powell B J, Baruah T, Bernstein N, Brake K, McKenzie R H, Meredith P & Pederson M R, *J Chem Phys*, 120 (2004) 8608.
46 Choi C H & Kertesz M, *J Phys Chem*, A 101 (1997) 3823.
47 Ataly Y, Avci D & Basoglu A, *J Struct Chem*, 19 (2008) 239.
48 Vijayakumar T, Hubert J I, Nair C P R & Jayakumar V S, *J Chem Phys*, 343 (2008) 83.
49 Xavier Assfeld & Rivail J L, *Chem Phys Lett*, 263 (1996) 100.
50 Scrocco E & Tomasi J, *Adv Quant Chem*, 11 (1979) 115.
51 Okulik N & Jubert A H, *Int Electron J Mol Des*, (2005) 4.
52 Chidangil S, Shukla M K & Mishra P C, *J Mol Model*, 4 (1998) 250.
53 Nagabalasubramanian P B, Periyandi S & Mohan S, *Spectrochim Acta*, 77 (2010) 150.